THE UNIVERSITY OF READING

An Upwind Scheme for the 2D Shallow Water Equations with Applications

by

P. Brufau

Numerical Analysis Report 11/97

DEPARTMENT OF MATHEMATICS

AN UPWIND SCHEME FOR THE 2D SHALLOW WATER EQUATIONS WITH APPLICATIONS

P. Brufau [1]
Institute for Computational Fluid Dynamics
Department of Mathematics
University of Reading, U.K.

December 5, 1997

[1]Mecánica de Fluidos. Centro Politécnico Superior. Universidad de Zaragoza.

Abstract

In this report a first order multidimensional upwind scheme is presented for the modelling of free surface flow in two dimensions. Free surface flow in channels is described mathematically by the Shallow Water equations. These equations are discretised using a finite volume approach on quadrilaterals and unstructured triangles. We describe an upwind scheme for hyperbolic conservation laws. The method is first order in both space and time. However, it is capable of handling complex flow domains, as we show in the simulation of a dam-break problem in an L-shaped channel, as well as different source terms such as those in a basin irrigation problem, and finally problems involving wetting/drying.

1 Introduction

Recently there has been considerable interest in modelling fluid flow in rivers and channels, much of which has come from the increased public awareness of pollution and environmental issues in relation to construction projects, such as coastal defences, water supply, treatment, drainage, irrigation and so on. The standard model equations are the Shallow Water equations (Abbott, 1992) which because of the complexity of the problems need to be solved numerically.

For this purpose we need a numerical scheme with the necessary features to handle both steady and transient flow conditions, capable of describing and incorporating complex topography, simulating both sub- and super-critical conditions, enabling inflow/outflow conditions to be specified at different points in the domain of interest, and finally allowing the wetting/drying of flood plains and river beds. In addition we would like to have a correct description of the physical problem, easy implementation, accuracy and speed of computation.

An important issue is the mesh, which should relate to the topology of the problem being considered; there are clearly difficulties associated with adapting a structured grid system to an irregular shape domain. For this reason we have used unstructured meshes, and a comparison between unstructured meshes based on quadrilateral and triangular cells has been carried out for an experimental test.

We have used the conservative form of the Shallow Water equations that permits a Riemann solver to be used within a finite volume formulation. This combination allows us to obtain solutions of complex problems on unstructured grids with good accuracy and resolution of extreme conditions such as hydraulic jumps.

The motivation of this work is to find a fast algorithm with a wide range of practical applicability. More specifically, the method:

- is based on the conservative form of the Shallow Water equations,
- uses a finite volume formulation with triangular and quadrilateral unstructured meshes depending on the geometry of the problem,
- employs an approximate Riemann solver to calculate the fluxes,
- is first order accurate in both space and time,
- has the flexibility to specify general boundary conditions, including the capacity to deal with wetting/drying conditions.

2 Governing equations

The two-dimensional Shallow Water equations that govern free surface flow in conservative form (Cunge, 1980) are

$$\frac{\partial \mathbf{U}}{\partial t} + \frac{\partial \mathbf{F}}{\partial x} + \frac{\partial \mathbf{G}}{\partial y} = \mathbf{H} \tag{2.1}$$

with

$$\mathbf{U} = \begin{pmatrix} h \\ hu \\ hv \end{pmatrix} , \mathbf{F} = \begin{pmatrix} hu \\ hu^2 + g\frac{h^2}{2} \\ huv \end{pmatrix} , \mathbf{G} = \begin{pmatrix} hv \\ huv \\ hv^2 + g\frac{h^2}{2} \end{pmatrix} , \mathbf{H} = \begin{pmatrix} 0 \\ gh(S_{0x} - S_{fx}) \\ gh(S_{0y} - S_{fy}) \end{pmatrix}$$

where $\mathbf{U}$ represents the vector of conservative variables, $\mathbf{F}$ and $\mathbf{G}$ are the convective fluxes in the x, y directions respectively, and $\mathbf{H}$ is the source term. In addition, h is the depth of water, u and v are the velocities in the x, y directions respectively, g is the acceleration due to gravity, S_{0x}, S_{0y} are the bed slopes and S_{fx}, S_{fy} the friction terms in the x, y directions.

For the friction term, the Manning equation has been used in the form

$$S_{fx} = \frac{n^2 u\sqrt{u^2+v^2}}{h^{\frac{4}{3}}} \quad , \quad S_{fy} = \frac{n^2 v\sqrt{u^2+v^2}}{h^{\frac{4}{3}}} \tag{2.2}$$

where n is the Manning coefficient.

3 The first order upwind scheme

3.1 Discretisation procedure

A cell centred finite volume method is formulated for equation (2.1) over a quadrilateral or triangular control volume with the dependent variables of the system represented as piecewise constants.

We can write the convective flux as $(\mathbf{F}, \mathbf{G})$ so equation (2.1) becomes

$$\frac{\partial \mathbf{U}}{\partial t} + \nabla \cdot (\mathbf{F}, \mathbf{G}) = \mathbf{H} \tag{3.1}$$

The integral form of (3.1) for a fixed area Ω is

$$\frac{\partial}{\partial t} \int_\Omega \mathbf{U} d\Omega + \int_\Omega \nabla \cdot (\mathbf{F}, \mathbf{G}) d\Omega = \int_\Omega \mathbf{H} d\Omega \tag{3.2}$$

and, applying the divergence theorem, we obtain

$$\frac{\partial}{\partial t} \int_\Omega \mathbf{U} d\Omega + \oint_S (\mathbf{F}, \mathbf{G}) \cdot \mathbf{n} dS = \int_\Omega \mathbf{H} d\Omega \tag{3.3}$$

where S is the boundary of the area Ω.

A finite volume approximation of the equations is the result of a discretisation of their integral form. We introduce a computational mesh that defines the finite volumes Ω_i where i is the index associated with the centroid of the cell in which we store the cellwise constant values of $\mathbf{U}$.

Equation (3.3) can then be replaced by

$$\frac{\partial \mathbf{U}_i}{\partial t} \Omega_i + \oint_{S_i} (\mathbf{F}, \mathbf{G}) \cdot \mathbf{n} dS = \mathbf{H}_i \Omega_i \tag{3.4}$$

because the mesh is fixed in time.

Equation (3.4) represents a system of ordinary differential equations in which we have yet to define the boundary integral. We approach this integral via a mid-point rule, i.e. the numerical flux is calculated at the mid-point of each edge, giving

$$\oint_{S_i} (\mathbf{F}, \mathbf{G}) \cdot \mathbf{n} dS = \sum_{k=1}^{NE} (\mathbf{F}, \mathbf{G})^*_{w_k} \cdot \mathbf{n}_{w_k} dS_{w_k} \tag{3.5}$$

where w_k represents the index of edge k of the cell, NE is the total number of edges in the cell (for a quadrilateral cell NE=4, and for a triangle NE=3). The vector $\mathbf{n}_{w_k}$ is the unit outward normal, dS_{w_k} is the length of the side, and $(\mathbf{F}, \mathbf{G})^*_{w_k}$ is the numerical flux.

3.2 Numerical Flux calculation: upwind differentiation

A characteristic of the Shallow Water system of equations, which is very useful when developing an unstructured finite volume scheme, is that they are rotationally invariant, enabling problems to be posed as locally one-dimensional. Evaluation of the numerical flux in equation (3.5) is carried out by a series of solutions local to the lines which make up the quadrilateral and triangle meshes. The Riemann problem is defined by the solutions on the left and right of the cell edges, as in the first order MUSCL scheme (Van Leer, 1977).

An important feature of the one-dimensional upwind schemes is the definition of the approximated flux jacobian, $\tilde{A}_{i+\frac{1}{2}}$, constructed at the edges of the cells. Once this matrix has been defined, the numerical flux (normal to the edge) is (Alcrudo, 1992)

$$\mathbf{F}^*_{i+\frac{1}{2}} = \frac{1}{2}\left[\mathbf{F}_{i+1} + \mathbf{F}_i - |\tilde{A}_{i+\frac{1}{2}}|(\mathbf{U}_{i+1} - \mathbf{U}_i)\right] \tag{3.6}$$

It is possible to achieve second order accuracy by defining better estimates of the values on the left $\mathbf{U}_L$ and right $\mathbf{U}_R$ of the cell edge (or internal and external values to the finite volume) and substituting them for $\mathbf{U}_{i+1}$ and $\mathbf{U}_i$ in equation (3.6), giving

$$\mathbf{F}^*_{i+\frac{1}{2}} = \frac{1}{2}\left[\mathbf{F}_R + \mathbf{F}_L - |\tilde{A}_{RL_{i+\frac{1}{2}}}|(\mathbf{U}_R - \mathbf{U}_L)\right] \tag{3.7}$$

The 2D numerical upwind flux in equation (3.5) is obtained by applying the expression (3.7) in a one-dimensional form to each edge of the computational cells, so that

$$(\mathbf{F},\mathbf{G})^*_{wk}\cdot\mathbf{n}_{wk}=\frac{1}{2}\left[((\mathbf{F},\mathbf{G})_R+(\mathbf{F},\mathbf{G})_L)_{wk}\cdot\mathbf{n}_{wk}-|\tilde{J}_{RL_{wk}}|(\mathbf{U}_R-\mathbf{U}_L)_{wk}\right] \tag{3.8}$$

Here $k=1,...,NE$, R and L denote right and left states respectively at the w_k edge, $(\tilde{J}_{RL_{wk}})$ represents the approximate jacobian of the normal flux vector and corresponds to $(\tilde{A}_{RL_{i+\frac{1}{2}}})$ used in the one-dimensional schemes.

$|\tilde{J}_{RL_{wk}}|$ is the matrix whose eigenvalues are the absolute values of the eigenvalues of the matrix $(\tilde{J}_{RL_{wk}})$ (Alcrudo, 1992). This matrix must satisfy the following conditions:

- $(\tilde{J}_{RL_{wk}})$ depends only on the $\mathbf{U}_R$ and $\mathbf{U}_L$ states,
- $(\mathbf{F}_R-\mathbf{F}_L)_{wk}=(\tilde{J}_{RL_{wk}})(\mathbf{U}_R-\mathbf{U}_L)_{wk}$,
- $(\tilde{J}_{RL_{wk}})$ has real and distinct eigenvalues and a complete set of eigenvectors,
- $(\tilde{J}_{RL_{wk}})=J(\mathbf{U}_R)=J(\mathbf{U}_L)\quad$ if $\quad\mathbf{U}_R=\mathbf{U}_L$

where

$$J=\frac{\partial(\mathbf{F},\mathbf{G})\cdot\mathbf{n}}{\partial\mathbf{U}}=\frac{\partial\mathbf{F}}{\partial\mathbf{U}}n_x+\frac{\partial\mathbf{G}}{\partial\mathbf{U}}n_y \tag{3.9}$$

The matrix $(\tilde{J}_{RL_{wk}})$ has the same shape as J but is evaluated at an averaged state given by the quantities $\tilde{\mathbf{u}}=(\tilde{u},\tilde{v})$ and $\tilde{c}$ which must be calculated as shown later. The eigenvalues are

$$\begin{aligned}\tilde{a}^1&=\tilde{\mathbf{u}}\cdot\mathbf{n}+\tilde{c}\\ \tilde{a}^2&=\tilde{\mathbf{u}}\cdot\mathbf{n}\\ \tilde{a}^3&=\tilde{\mathbf{u}}\cdot\mathbf{n}-\tilde{c}\end{aligned} \tag{3.10}$$

where $\tilde{\mathbf{u}}\cdot\mathbf{n}=\tilde{u}n_x+\tilde{v}n_y$, and the eigenvectors are

$$\tilde{e}^1=\begin{pmatrix}1\\ \tilde{u}+\tilde{c}n_x\\ \tilde{v}+\tilde{c}n_y\end{pmatrix}\quad,\quad\tilde{e}^2=\begin{pmatrix}0\\ -\tilde{c}n_y\\ \tilde{c}n_x\end{pmatrix}\quad,\quad\tilde{e}^3=\begin{pmatrix}1\\ \tilde{u}-\tilde{c}n_x\\ \tilde{v}-\tilde{c}n_y\end{pmatrix} \tag{3.11}$$

Once we have calculated these eigenvalues and eigenvectors, we can decompose the difference in the vector $\mathbf{U}$ across a grid edge as a sum of the eigenvectors as

$$\mathbf{U}_R - \mathbf{U}_L = \sum_{m=1}^{3} \alpha_{RL}^m \tilde{e}_{RL}^m \tag{3.12}$$

where

$$\begin{aligned} \alpha_{RL}^{1,3} &= \frac{\delta h_{RL}}{2} \pm \frac{1}{2\tilde{c}} \left[\delta(hu)_{RL} n_x + \delta(hv)_{RL} n_y - \tilde{u}\mathbf{n}\delta h_{RL} \right] \\ \alpha_{RL}^{2} &= \frac{1}{\tilde{c}} \left[\left(\delta(hv)_{RL} - \tilde{v}\delta h_{RL} \right) n_x - \left(\delta(hu)_{RL} - \tilde{u}\delta h_{RL} \right) n_y \right] \end{aligned} \tag{3.13}$$

and δ denotes

$$\delta h_{RL} = h_R - h_L$$

Enforcing the second condition of the matrix $(\tilde{J}_{RL_{wk}})$ we can obtain the following expressions for $\tilde{u}$, $\tilde{v}$, and $\tilde{c}$.

$$\tilde{u} = \frac{\sqrt{h_R} u_R + \sqrt{h_L} u_L}{\sqrt{h_R} + \sqrt{h_L}} \quad , \quad \tilde{v} = \frac{\sqrt{h_R} v_R + \sqrt{h_L} v_L}{\sqrt{h_R} + \sqrt{h_L}} \quad , \quad \tilde{c} = \sqrt{\frac{g}{2}(h_R + h_L)}$$

For a first order scheme the values of the variables at the left and right side of each wall of the cell are taken to be $\mathbf{U}_L = \mathbf{U}_i$ and $\mathbf{U}_R = \mathbf{U}_j$, the solution at the centres of adjacent cells. As we have said before, second order accuracy can be achieved using an upwind weighted linear interpolation function (Berzins, Ware, 1995) amongst others.

3.3 Time integration

Once the approximate jacobian matrix has been constructed, equation (3.8) provides the numerical flux normal to each edge of the computational cells. We can now substitute it into the equation (3.5), so that equation (3.4) can be written as

$$\frac{\partial \mathbf{U}_i}{\partial t} = \frac{-1}{\Omega_i} \sum_{k=1}^{NE} (\mathbf{F}, \mathbf{G})_{w_k}^* \cdot \mathbf{n}_{w_k} dS_{w_k} + \mathbf{H}_i \tag{3.14}$$

which is an ordinary differential equation and can be integrated by standard methods. We have used in all our cases a forward Euler time integration, although second order accuracy in time can be easily achieved by evaluating this integral using a Predictor-Corrector algorithm.

The stability criterion is difficult to obtain because the algorithm is non-linear. However, in the case of the linearised equation of the form

$$\frac{\partial u}{\partial t} + a\frac{\partial u}{\partial x} + b\frac{\partial u}{\partial y} = 0 \tag{3.15}$$

with constants $a, b > 0$, using an upwind algorithm in finite volume differencing in a uniform mesh, the time step is limited by (Barley, 1988),

$$\delta t \leq \left(\frac{a}{\delta x} + \frac{b}{\delta y}\right)^{-1} \tag{3.16}$$

We have adopted this stability criterion, adapting it to the non-linear finite volume context as

$$\delta t \leq min\left[\frac{d_{ij}}{2(\sqrt{u^2+v^2}+c)_{ij}}\right] \tag{3.17}$$

where d_{ij} is the distance between the centroid of the cell i and its neighbours j.

4 Boundary conditions

The idea of using a Riemann solver to calculate the flux at the face of a cell can be exploited in the description of boundary conditions. The variables are stored at the centre of each cell and the boundary conditions are applied through the flux across the edges. The imposed conditions at the boundaries combined with equations obtained from characteristics theory give sufficient information for the boundary flux to be calculated.

We have applied characteristics theory (Alcrudo, 1992) in two dimensions, the procedure consisting of the approximation of the bicharacteristics that go through the boundary points. Assuming that we can neglect the source terms and that the flux has a frontal behaviour we arrive at the following compatibility relations:

$$\frac{D}{Dt}(\mathbf{u}\cdot\mathbf{n}\pm 2c)=0 \tag{4.1}$$

$$\frac{\delta}{\delta t}(\mathbf{u}\cdot\mathbf{t})=0 \tag{4.2}$$

where

$$\begin{aligned}\mathbf{u}\cdot\mathbf{n}&=un_x+vn_y\\ \mathbf{u}\cdot\mathbf{t}&=vn_x-un_y\end{aligned} \tag{4.3}$$

and

$$\frac{D}{Dt}=\frac{\partial}{\partial t}+(u\pm cn_x)\frac{\partial}{\partial x}+(v\pm cn_y)\frac{\partial}{\partial y} \tag{4.4}$$

$$\frac{\delta}{\delta t}=\frac{\partial}{\partial t}+u\frac{\partial}{\partial x}+v\frac{\partial}{\partial y} \tag{4.5}$$

Sometimes it is not necessary to use all the equations, depending on the boundary conditions imposed, the number being determined by the normal velocity through the boundary. Some of the possible situations are:

- Supercritical inflow: all the variables must be imposed.
- Subcritical inflow: two variables must be imposed.
- Supercritical outflow: none of the variables must be imposed.

- Subcritical outflow: one variable must be imposed.

When the boundary is a solid wall the normal velocity is zero, so it is necessary to use the above relations with the condition $\mathbf{u} \cdot \mathbf{n} = 0$. Special boundary conditions for the irrigation problem will be discussed in the next sections.

Once we have imposed the boundary conditions on the cell edges and they have been combined with the appropiate compatibility relations, which can be different in each case, we calculate the normal flux across these edges and we obtain the contribution in the updating of the variables at the centre of the cell.

5 Applications

5.1 Dam-break problem in an L-shaped channel

In order to demonstrate the flexibility of the algorithm, a dam-break problem in an L-shaped channel is considered. Some comparisons between results on quadrilateral and triangular unstructured meshes with experimental measurements are shown. This is a common problem in hydraulic flow simulations (Glaister, 1993). The type of the flow will reveal any weakness in relation to how well a particular strategy deals with combined sub- and super-critical flow.

The flow domain, detailed in Figure 1, consists of a square reservoir that contains a wall to separate it from the L-shaped channel. The initial conditions are zero flow with 0.2m depth to the left and 0.01m depth to the right of the wall. The resultant flow is clearly two-dimensional, highly non-linear and possibly transcritical.

All boundaries are treated as solid non-slip walls except the outflow which is considered supercritical. The Manning coefficient is 0.0095 and the bed slope is zero. The number of cells in the quadrilateral mesh is 3812, and in the triangular mesh is 2954. The quadrilateral and the triangular meshes are shown in Figures 1-2.

Comparisons of the time evolution of the depth of water are made at the points P1, P2, P3, P4, P5 and P6, whose respective coordinates are (1.2m,1.2m), (2.75m,0.7m), (4.25m,0.7m), (5.75m,0.7m), (6.55m,1.5m), (6.55m,3m) and are shown with the experimental data in Figures 3-8. The experimental data were obtained from the 3rd Meeting of the Working Group on Dam-break Modelling (Brussels, June 1997) in which we participated actively.

It can be seen from the graphs that the triangular cell mesh is more robust than the quadrilateral one, although both give very similar results. Perhaps this is due to the number of edges involved in computing the numerical flux. If the domain is regular, either square or rectangular, the quadrilateral cell mesh gives better results than the triangular one.

As we expected, the worst results are obtained at point P5, after the corner of the channel. This is the critical point in the test. On the other hand, the arrival of the advancing front is accurately captured in all the points.

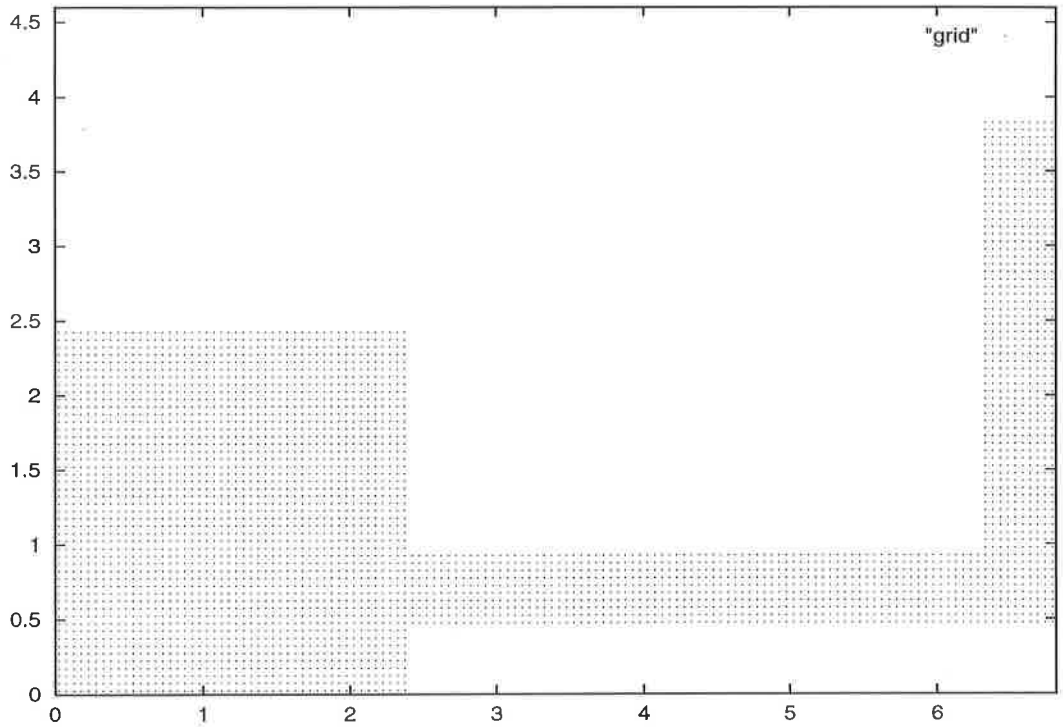

Figure 1: Geometry of the test and the quadrilateral structured mesh used in the x,y coordinates.

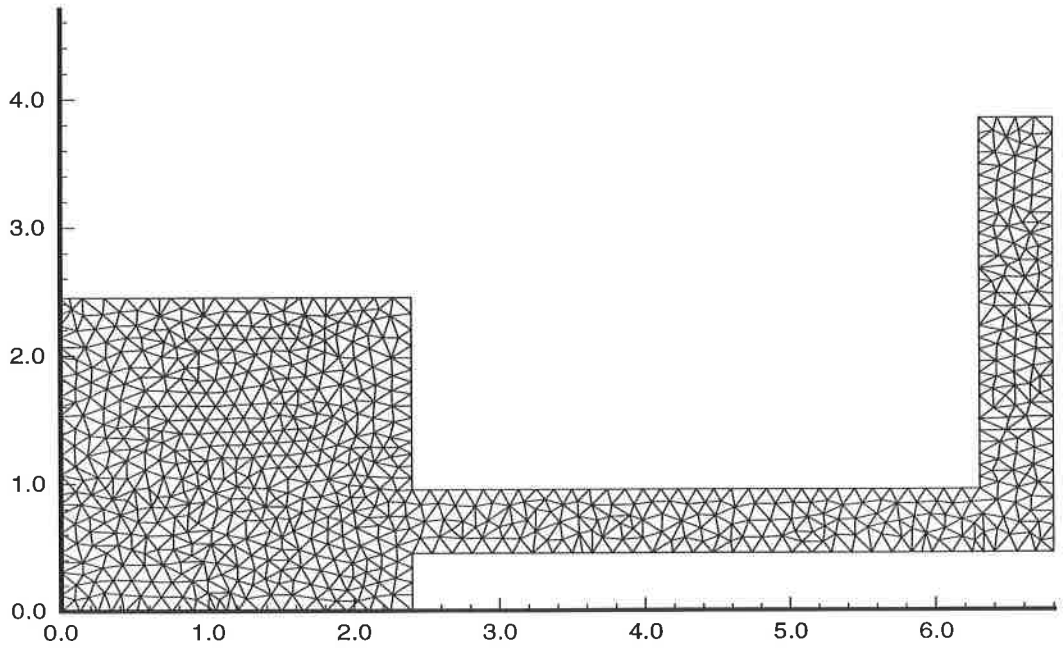

Figure 2: Geometry of the test and the triangular unstructured mesh used in the x,y coordinates.

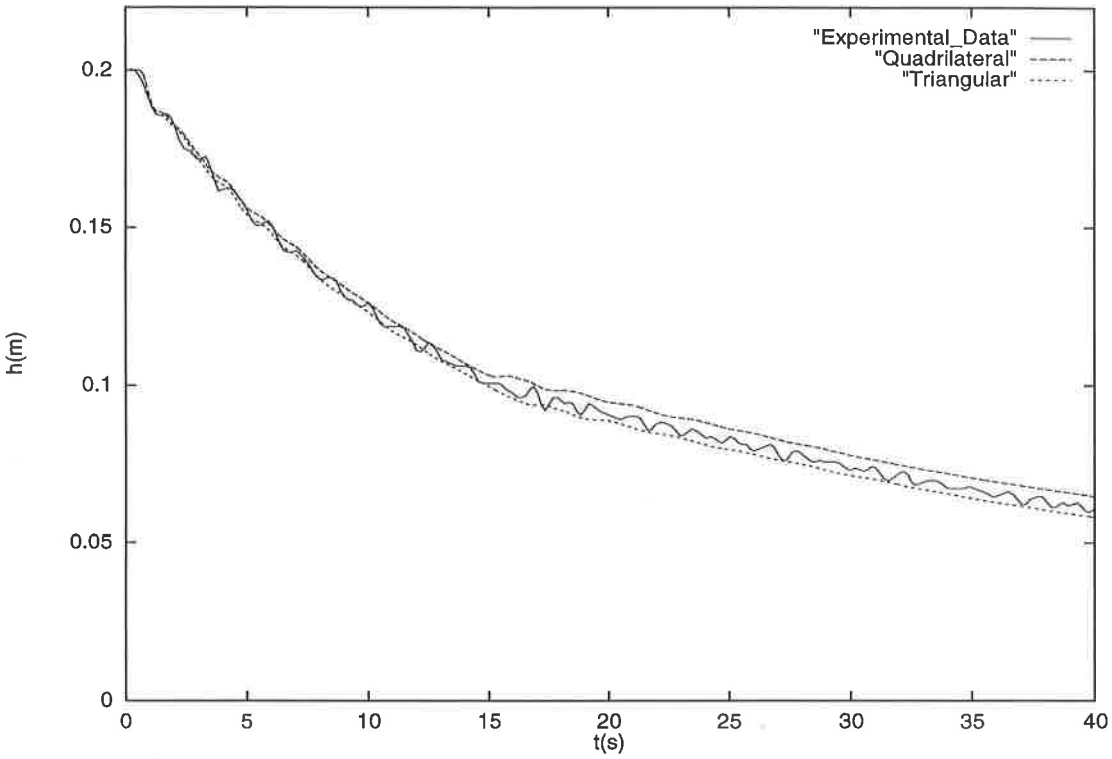

Figure 3: Time evolution of the depth of water at the point P1

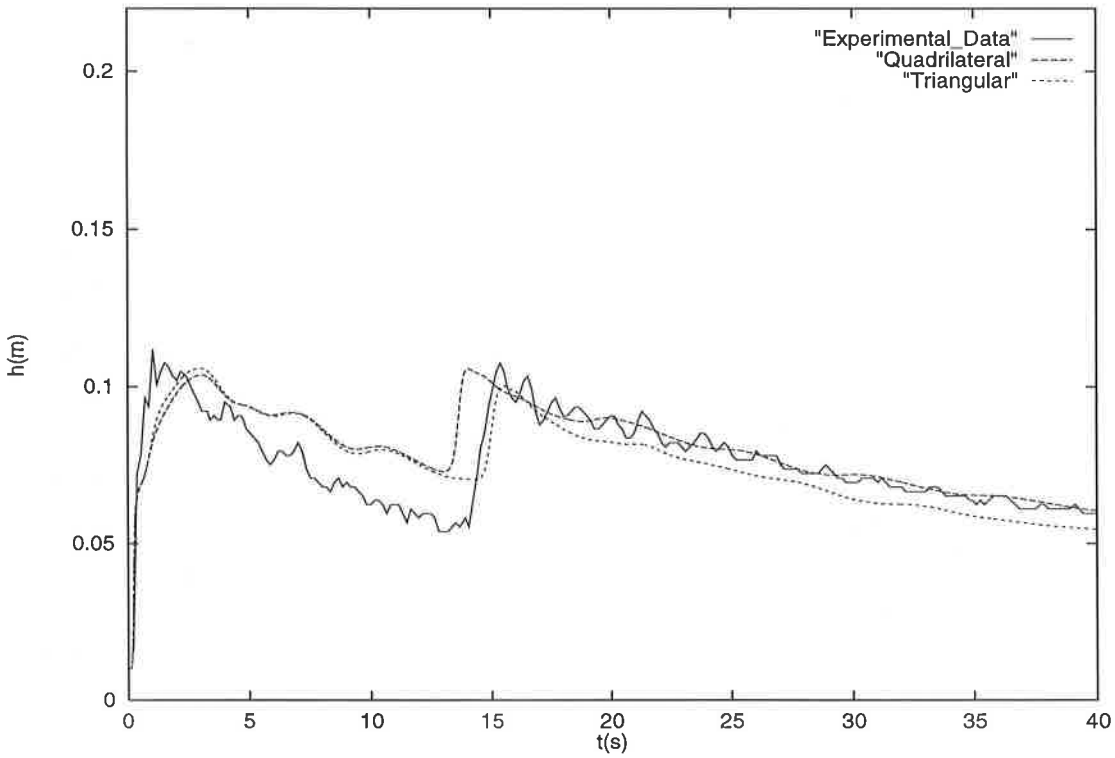

Figure 4: Time evolution of the depth of water at the point P2

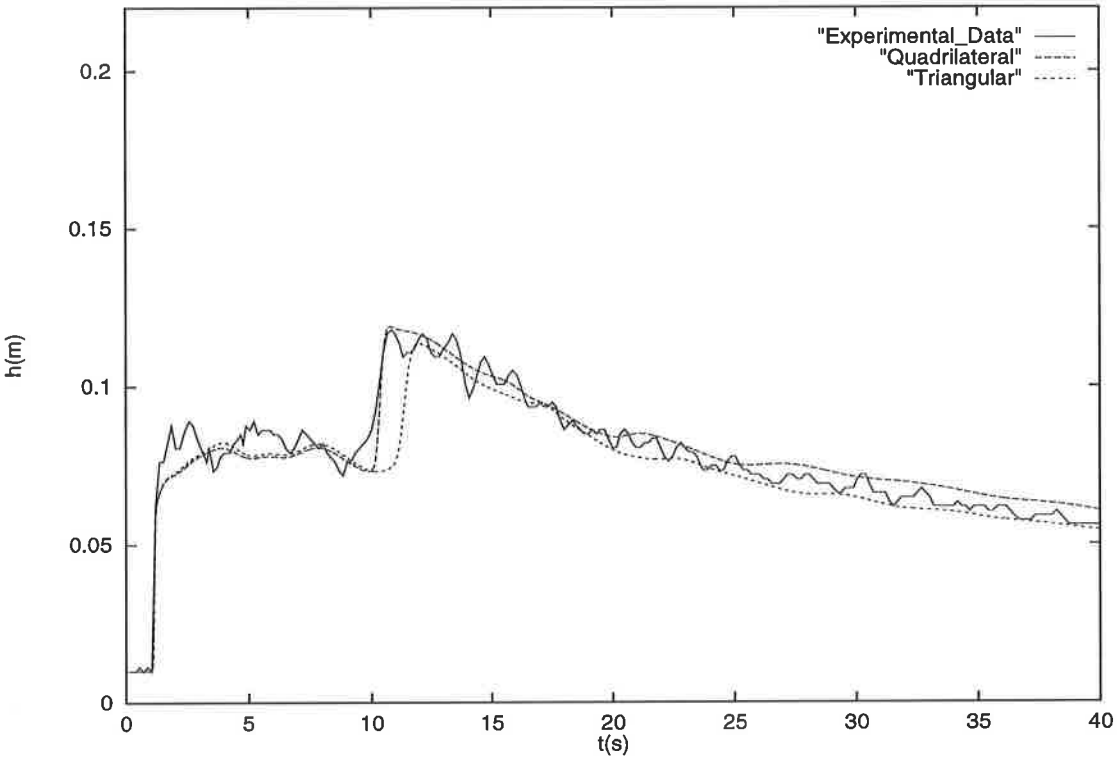

Figure 5: Time evolution of the depth of water at the point P3

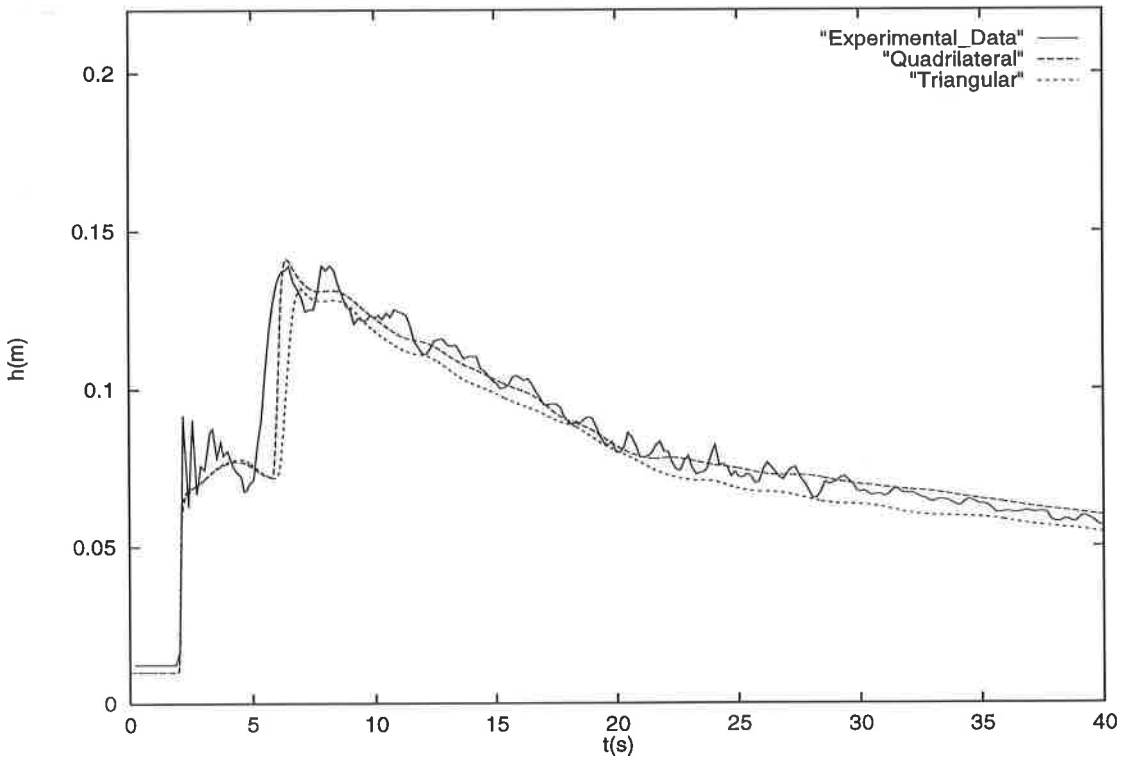

Figure 6: Time evolution of the depth of water at the point P4

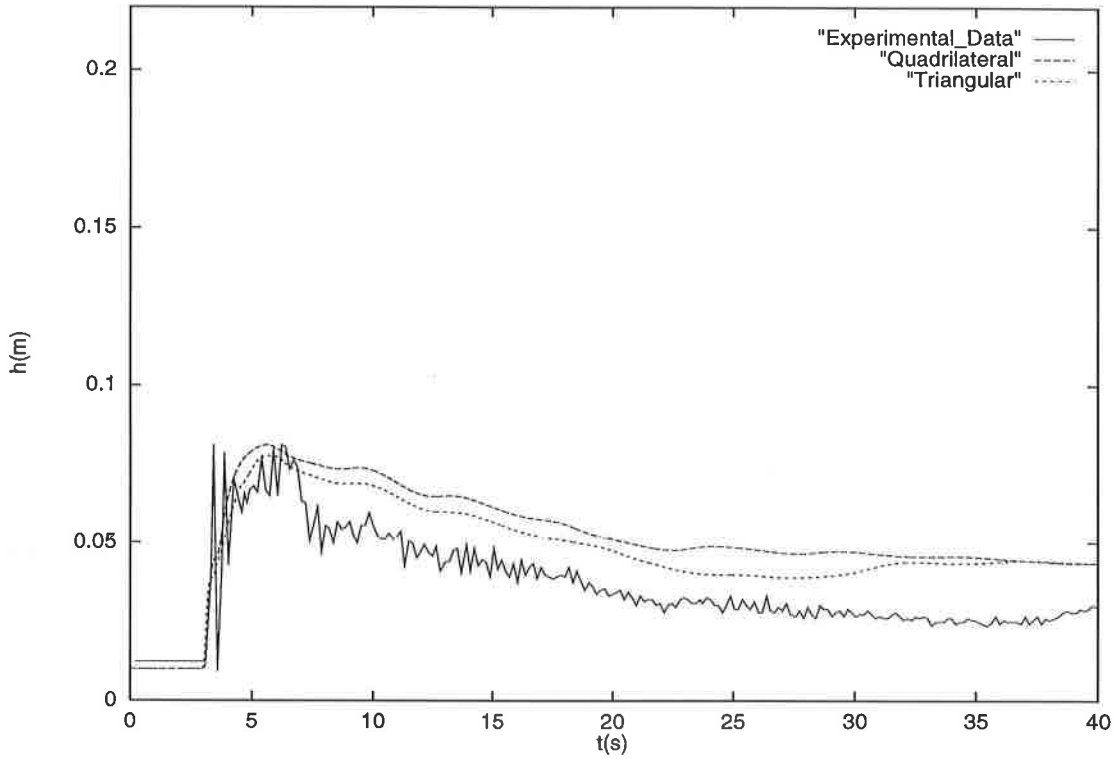

Figure 7: Time evolution of the depth of water at the point P5

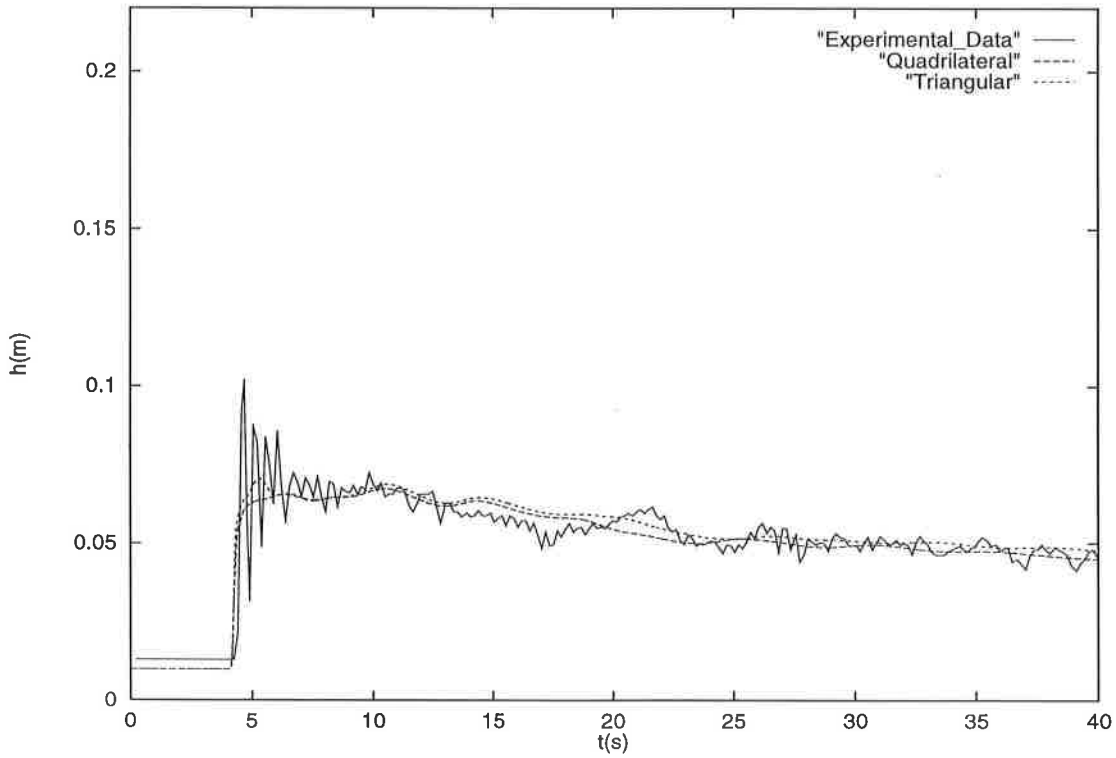

Figure 8: Time evolution of the depth of water at the point P6

5.2 Infiltration

Surface irrigation is the oldest and most extensively used irrigation method in agriculture. It has the distinguishing characteristic that water is distributed over the field by its internal pressure. The efficiency of surface irrigation systems is typically low. Surface irrigation systems are commonly modelled using a one-dimensional analysis. However, in many basin irrigation configurations the 1D hypothesis cannot be justified, especially if the geometry of the field is irregular or if the water does not enter the field continuously along one of its sides.

The need for a two-dimensional model is therefore justified by its capability to deal with irregular field shapes, point or linear water inflow, and multiple inflow points.

The governing equations are the Shallow Water equations, with three new source terms, i, D_{lx} and D_{ly}. The set of equations are the ones described in section 2, equation (2.1). The only change that has been made is in the source term $\mathbf{H}$ that now has the form

$$\mathbf{H} = \begin{pmatrix} -i \\ gh(S_{0x} - S_{fx}) + D_{lx} \\ gh(S_{0y} - S_{fy}) + D_{ly} \end{pmatrix} \tag{5.1}$$

where i is the infiltration rate and D_{lx}, D_{ly} account for the momentum transfer associated with seepage outflow in the x, y directions (Playán, 1992). The infiltration rate i can be computed using the empirical Kostiakov-Lewis equation,

$$i = ka\tau^{a-1} + f_0 \tag{5.2}$$

where τ is the opportunity time expressed in minutes, k and f_0 are coefficients determined by experimental measures and a is an exponent specified by the experiment too. The time integrated form of equation (5.2) provides the expression for z, the infiltrated depth of water in the field.

The following approximations are introduced to account for the momentum transfer due to seepage outflow (Akanbi, Katopodes, 1985):

$$D_{lx} = \frac{1}{2}ui \tag{5.3}$$

$$D_{ly} = \frac{1}{2}vi \tag{5.4}$$

Initial conditions

Since the numerical procedure requires all depths to be greater than zero to avoid undefined terms, a small positive value of 10^{-8}m is initially assigned to the depth of flow at all the cells of the domain. The same value is used to initialize u and v. This approximation means that the time step, normally chosen so that the CFL number satisfies the stability criterion, is very large, and so it must be reduced to allow the accurate evolution of water in the field.

Boundary conditions

Two types of boundary conditions have been implemented corresponding to different irrigation practices. A description of each type follows.

- Corner inflow: this simulates flooding of the rectangular domain from a point source located in one of its corners. Values of the three variables h, u, v are imposed on the cell edges.
- Line inflow: this represents a line source along a straight boundary of the domain, for example an overflowing ditch or several point sources located close to each other along the side of a basin. In this case we impose

$$u = \frac{Q}{N \cdot d \cdot h}$$

$$v = 0$$

where N is the number of inflow cells, d is the length of the edge of each cell and Q is the total discharge assigned to the inflow boundary condition.

The initial depth associated with each of the boundary cells involved in the inflow domain is computed from

$$h = 1.05 \left(\frac{Q^2}{g} \right)^{\frac{1}{3}}$$

which corresponds to the critical depth increased by 5% to ensure subcritical flow conditions at the inflow.

Advance and infiltration

A procedure has been introduced to ignore all flow depths smaller than a certain user-defined threshold, in our case 0.001m, that is the minimum flow depth considered as part of the advancing front and which allows infiltration to start. Every time

the depth of flow is computed for a cell, the program checks the validity of this new value. If it is smaller than the depth assigned as initial condition, it is reset to this value again. If the depth is greater than the threshold, irrigation will begin at the next time step.

Friction terms

Due to the small initial values for the variables h, u, and v and the high value of the Manning coefficient required to take in account the vegetation in the field, the friction terms become very strong. We have studied two possibilities to avoid this problem; the first is to ignore the friction terms when the depth of water is smaller than the threshold, while another more sophisticated approach is to treat the source terms in a semi-implicit form. The latter option is the one adopted in our case, although there is also the possibility of treating the source terms in an upwind way.

In the approximation that we have made, the friction terms are calculated in the following way: we change the calculation of the source terms vector **H** from equation (5.1) to

$$\mathbf{H} = \begin{pmatrix} -i \\ gh(S_{0x} - (1-\theta)S_{fx})^n - \theta(ghS_{fx})^{n+1} + D_{lx} \\ gh(S_{0y} - (1-\theta)S_{fy})^n - \theta(ghS_{fy})^{n+1} + D_{ly} \end{pmatrix} \tag{5.5}$$

where n indicates the time level in which we are calculating the variables and $n+1$ is the next time level where we update the variables. θ is a parameter that accounts for the implicitness of the treatment of the source terms in the equation and can take any value in the interval [0,1]. We have chosen $\theta = 0.5$ for the first numerical test and $\theta = 0.8$ for the second one.

Numerical test for the first field

A rectangular basin, 465m long by 100m wide, with an area of 46500m^2 is considered, irrigated from one of its 100m sides (Playán, 1992). Water flow in this test is basically one-dimensional. The number of cells in the mesh was 1860. The bed slope is zero. The infiltration parameters estimated in the experiment are:

$$\begin{aligned} k &= 0.00893 m/min^a \\ a &= 0.406 \\ f_0 &= 0.0 m/min \end{aligned}$$

A value of 0.1 is estimated for the Manning coefficient. The field is irrigated with a constant discharge of 0.183m^3/s. The field test consists of observations

of the advancing front over the field and the advance of the infiltrated depth of water.

Figure 9 presents the overland and infiltrated flow profiles at time=3h. We compared the results with the experimental data (Playán, 1992) but there was no agreement.

The advancing front moves faster in our case, reaching 325m in the y direction of the field, while the front in the results of Playán only reaches 200m at the same time. Besides that, the amount of infiltrated water is greater in the Playán results, the maximum depth of infiltrated water being 0.05 while our results give 10% less.

We had a lot of problems with the initial depth of water, set to 10^{-8}m instead of zero. The variables h, u and v are very small, which produce a large time step with fixed CFL. We therefore had to change the way of calculating the time step, decreasing the CFL value. Another important problem was the treatment of the friction terms as explained in the above section.

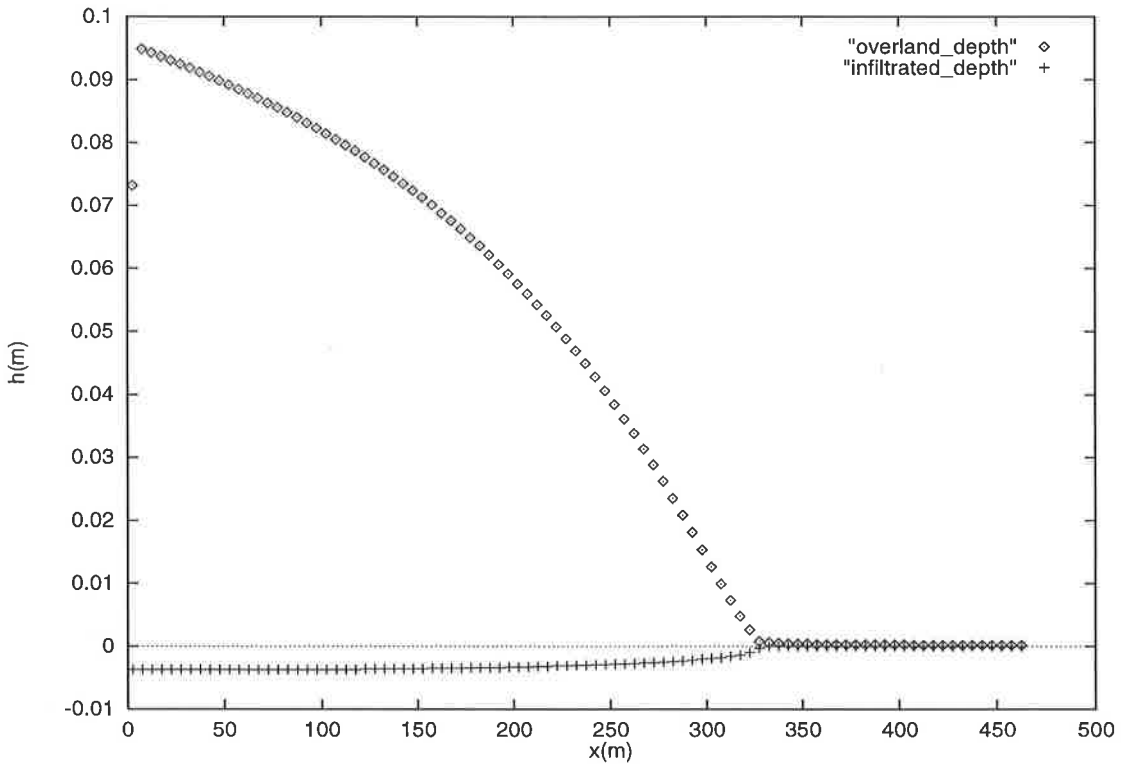

Figure 9: Overland and infiltrated depth of water in the field at time 3h.

Numerical test for the second field

This test was developed to illustrate the capability of the code to deal with two simultaneous corner inflows in a square field with an area of 10.000m^2. The number of cells in the mesh was 400.

The first inflow was located at the northwest corner, with a constant discharge of 0.1m^3/s. The turn-out time was 0min, and the cut-off time was 30min. The second inflow was located at the northeast corner, with a constant discharge of 0.1m^3/s. The turn-out time was 10min and the cut-off time was 40min. The applied infiltration parameters were:

$$k = 0.00324 m/min^a$$
$$a = 0.568$$
$$f_0 = 0.000174 m/min$$

The Manning coefficient was set to 0.04 and the bed slope was zero. Figures 10-17 show the results of the simulation at times 1min, 5min, 10min and 15min. The figures represent overland water surfaces and infiltrated water surfaces.

We tried to compare this test with the experimental measures (Playán, 1992) but without any success. Although at the first time steps the depth of water over the field of the advancing front are the same, the water infiltrated is greater in our case. This leads to another problem because now we have negatives depths of water and we have no way of dealing with them.

At time 15min the overland depth of water seems to be in good agreement with the Playán results, but this does not occur with the infiltrated depth of water.

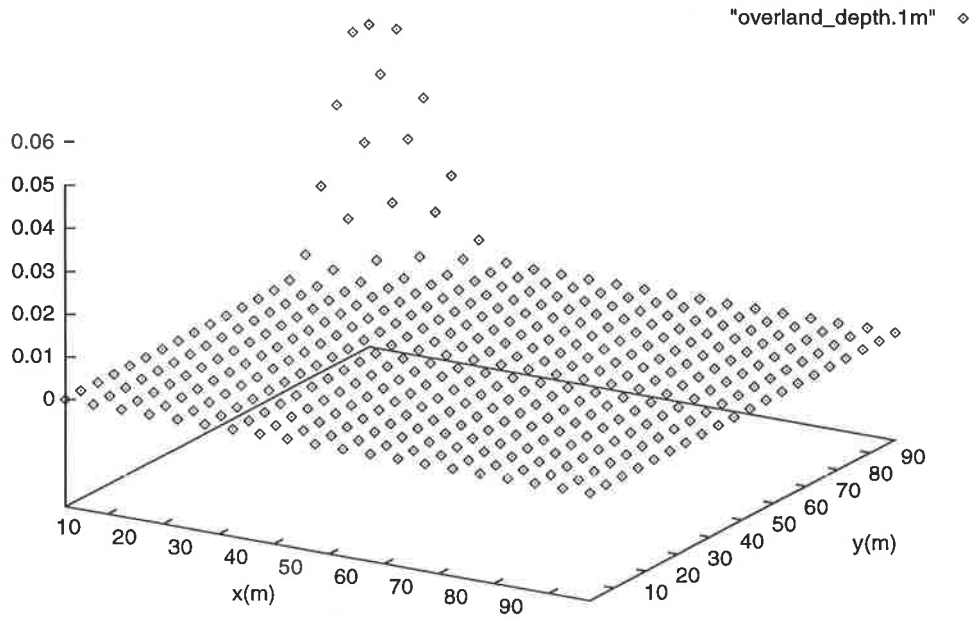

Figure 10: Overland surface of water in the field at time 1min.

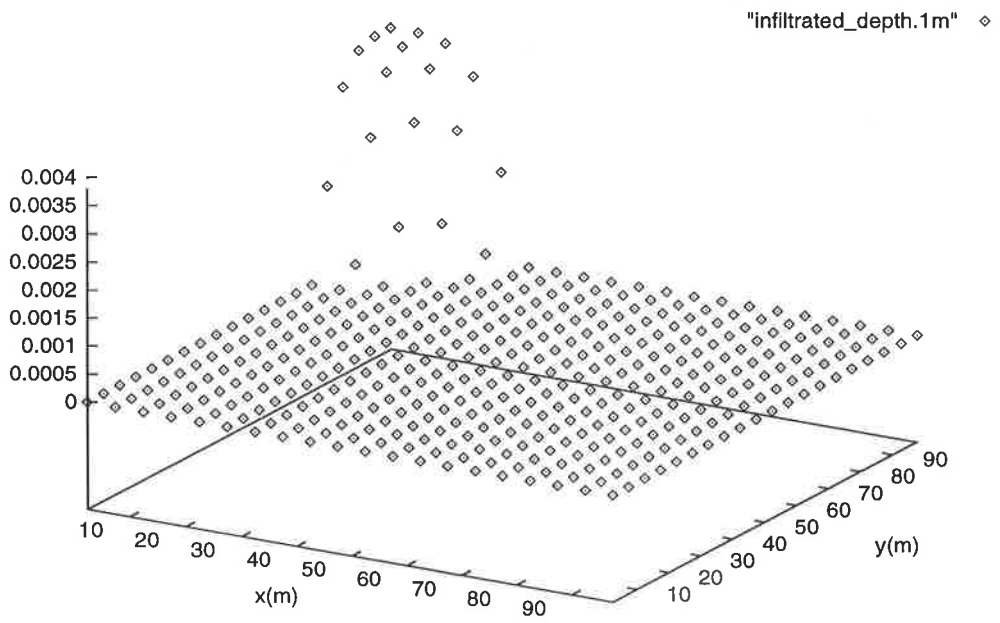

Figure 11: Infiltrated surface of water in the field at time 1min.

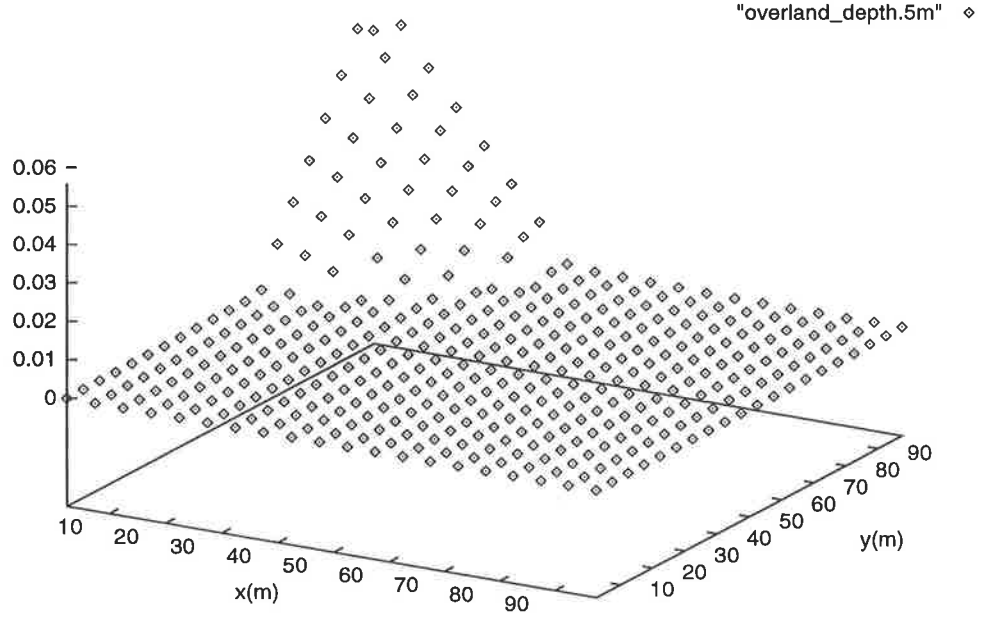

Figure 12: Overland surface of water in the field at time 5min.

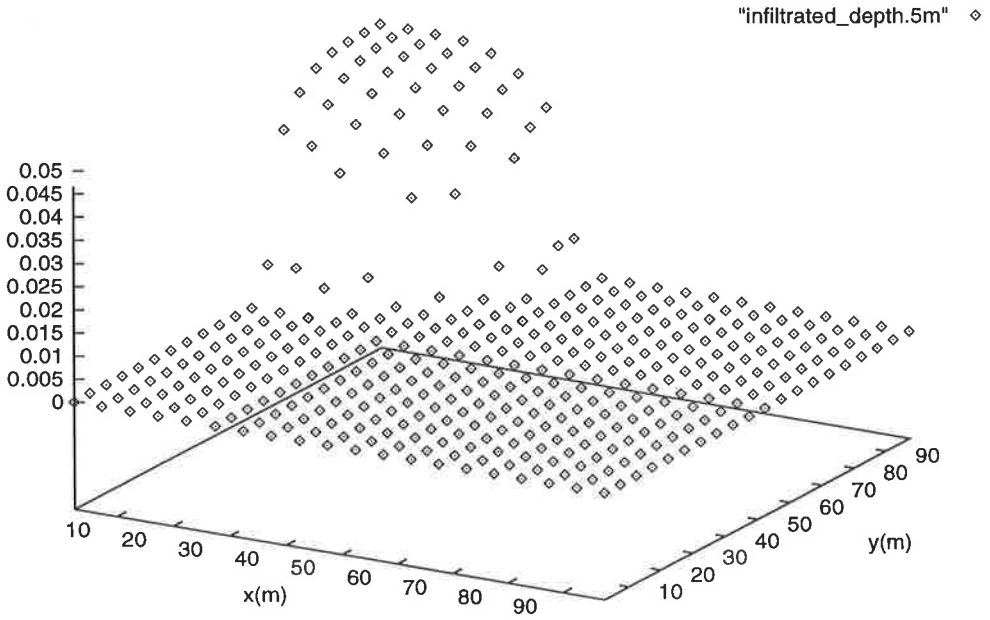

Figure 13: Infiltrated surface of water in the field at time 5min.

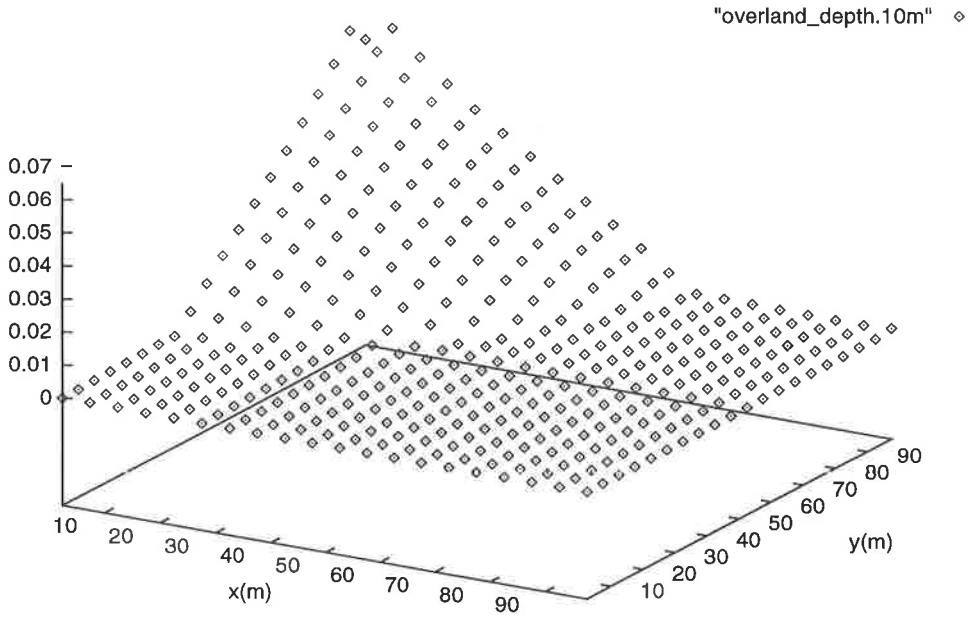

Figure 14: Overland surface of water in the field at time 10min.

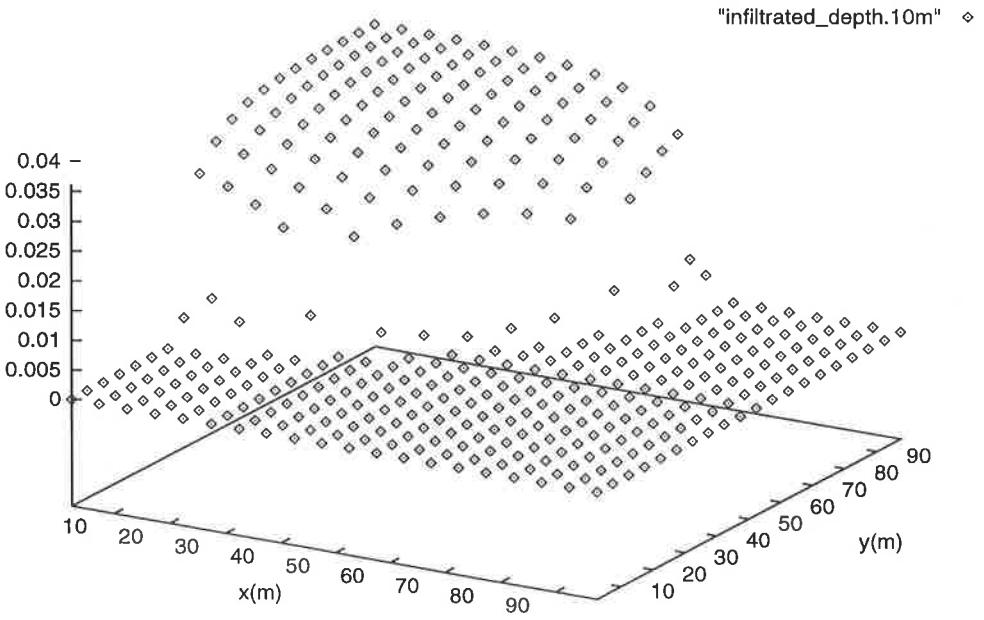

Figure 15: Infiltrated surface of water in the field at time 10min.

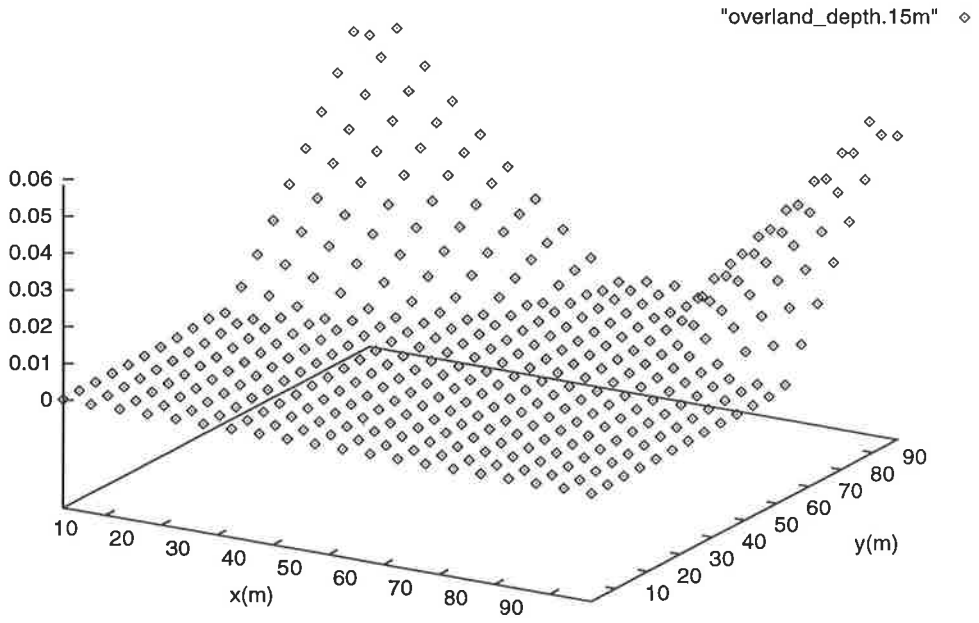

Figure 16: Overland surface of water in the field at time 10min.

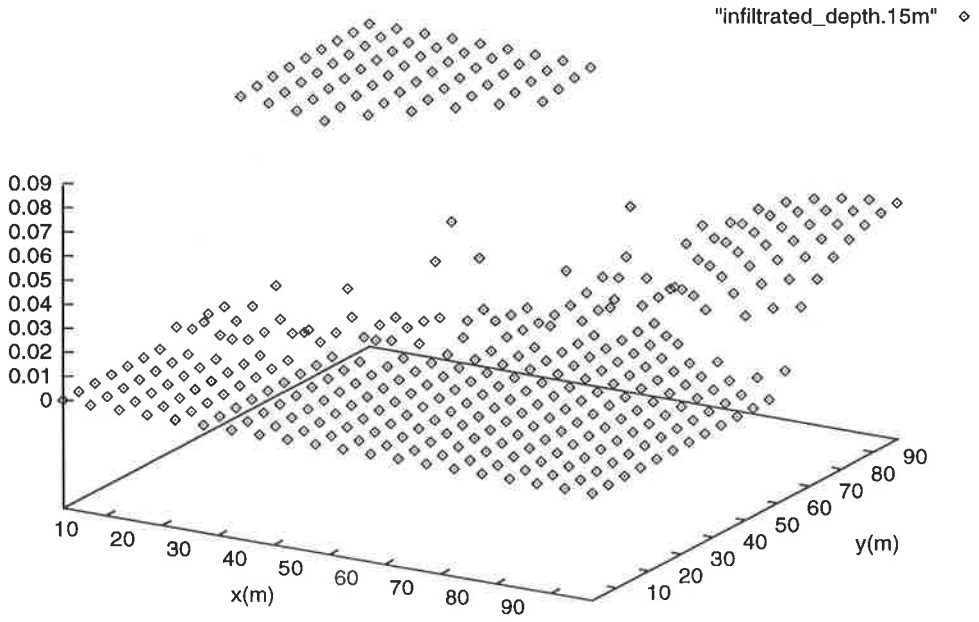

Figure 17: Infiltrated surface of water in the field at time 10min.

5.3 Wetting and drying

In practical two dimensional river flows, there exist boundaries at which the water depth approaches zero, so wetting/drying occurs. Clearly, an inadequate treatment of this boundary condition will affect the accuracy of the solution.

The approximate procedure used in this work is to examine the solution depth in each cell and proceed in a different way depending on the topography, the hydraulic conditions, the neighbouring cells and the cell we are examining in each time step. There follows the definition of time-dependent internal boundaries (Bento, 1996)

Three different situations can occur, and in each of them we have to impose additional conditions, without using the Shallow Water equations directly. These situations are named as: dry cell, high point and low point.

The first situation, **dry cell**, occurs when there is no water in any of the surrounding cells in the computational directions. In fact, this condition is satisfied when the depth of water in a cell and in its neighbours is less than a threshold, which in our case has been set to 0.001m. Then the conditions of a dry cell are

$$h_i = 0.0$$
$$h_j = 0.0$$

where i is the index of the cell we are examining and j is the index of any neighbouring cell.

In this case, the model sets the variables, h, u, v to zero in the cell, without allowing the upwind scheme to model the Shallow Water equations. With this condition, we speed up the computation in the regions where there is no water and at the same time avoid the anomalous appearance of water in cells or the appearance of negative depths of water.

The second situation, **high point**, occurs when the depth of water in the cell that we are examining is zero and the height of the bed is greater than the height of the water in its neighbouring cell. In this case we adopt the same solution as the one taken in the dry cell case. The conditions of a high point are

$$h_i = 0.0$$
$$z_i > h_j + z_j$$

The third situation, **low point**, is produced when the height of the bed in the neighbouring cell is greater than the height of the water in the cell under study. In this case, it is considered that there is a solid wall in that direction, so the flux must be reflected, and the upwind scheme is applied. The conditions of a low point are

$$h_i \neq 0.0$$
$$z_j > h_i + z_i$$

The model calculates the depth of water and the velocities in the x, y directions in each cell and at every time step, verifying at each point whether the upwind scheme can be applied or not.

Numerical test

A channel with trapezoidal cross section is considered. We assume that there is no bed slope in the x direction and the trapezoidal shape is achieved by imposing a certain bed depth, varying in the y direction, in some of the cells of the domain, which is a square field of 100m width and 100m length. The number of cells in the mesh was 400.

It is assumed for simplicity that there are no friction terms and that the initial condition is 0.3m depth of water and zero velocities in both directions. We impose a constant discharge at the inflow of $0.1\text{m}^3/\text{s}$.

In Figures 18-20 the depth of water is shown for different cross sections at 2.5m, 47.5m, and 97.5m of the channel at different times: 0s, 1s, 5s, 10s, 20s, and 30s.

In Figures 21-23 we show the time evolution of the depth of water in a dry cell that is suffering wetting/drying (cell1), its closest cell (cell2) and the next totally wet cells (cell3 and cell4) on one of the sides of the channel (the other side is symmetric) at the three cross sections specified above.

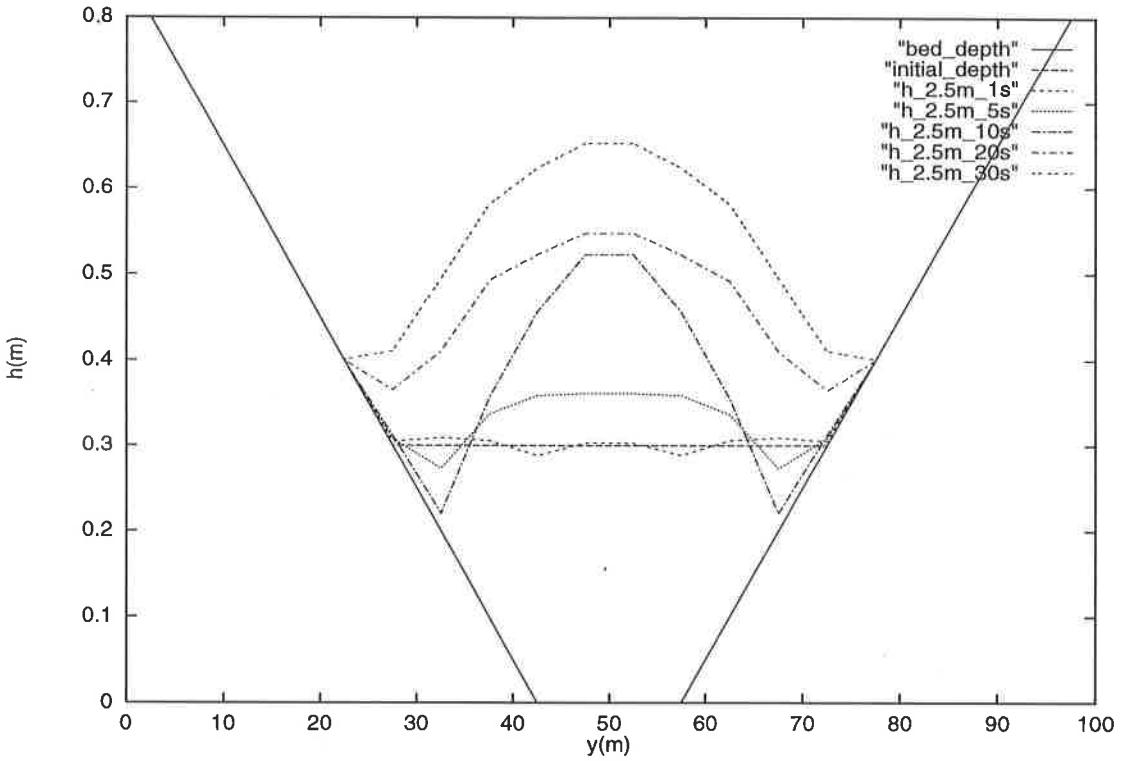

Figure 18: Depth of water profile in a cross section situated at 2.5m at different times.

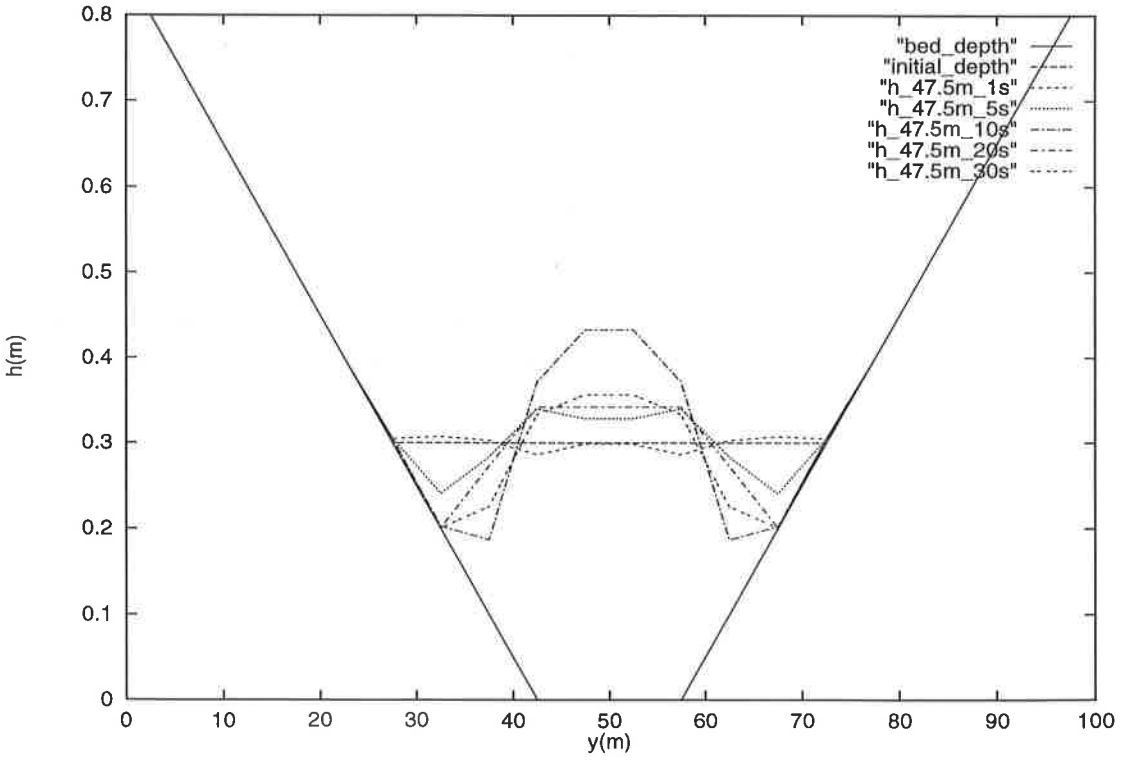

Figure 19: Depth of water profile in a cross section situated at 47.5m at different times.

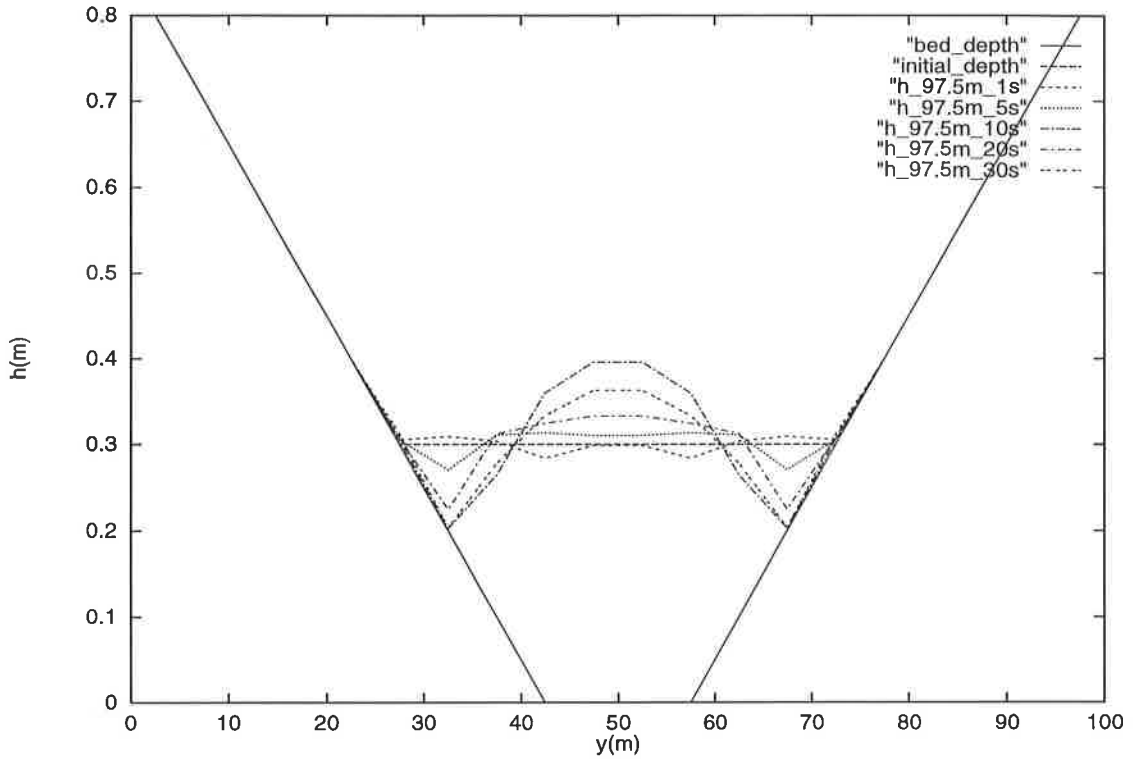

Figure 20: Depth of water profile in a cross section situated at 97.5m at different times.

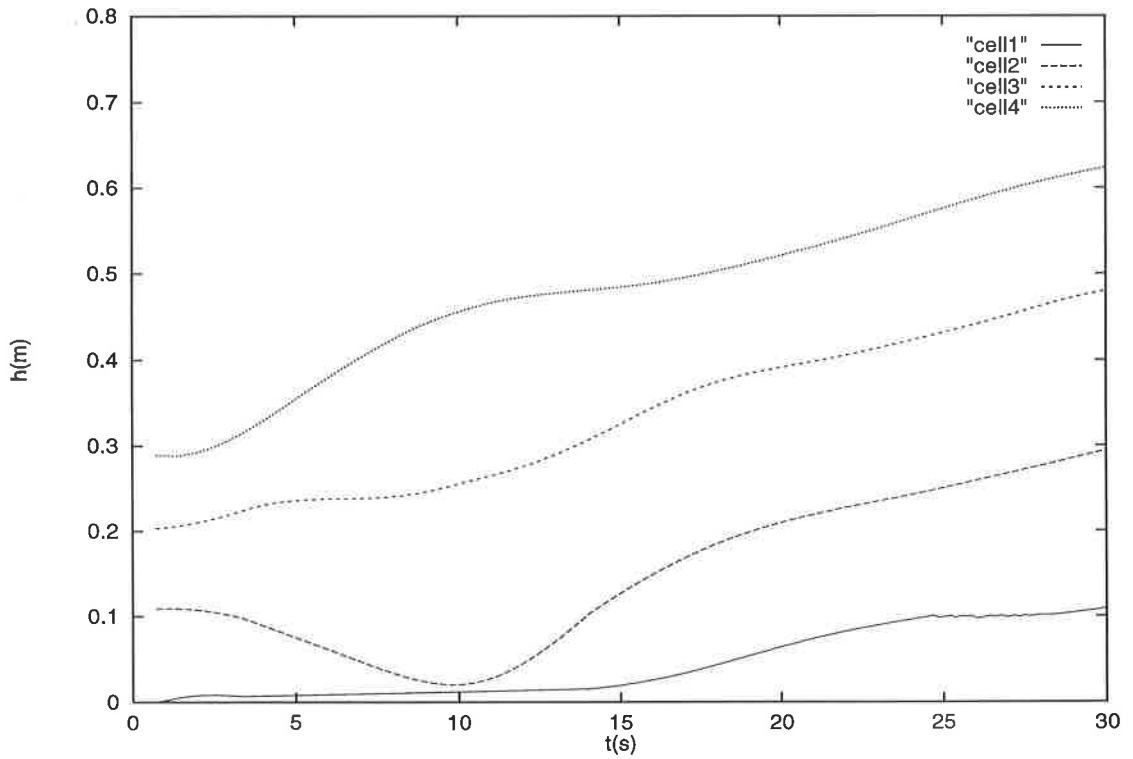

Figure 21: Time evolution of the depth of water in cell1, cell2, cell3 and cell4 in a cross section situated at 2.5m.

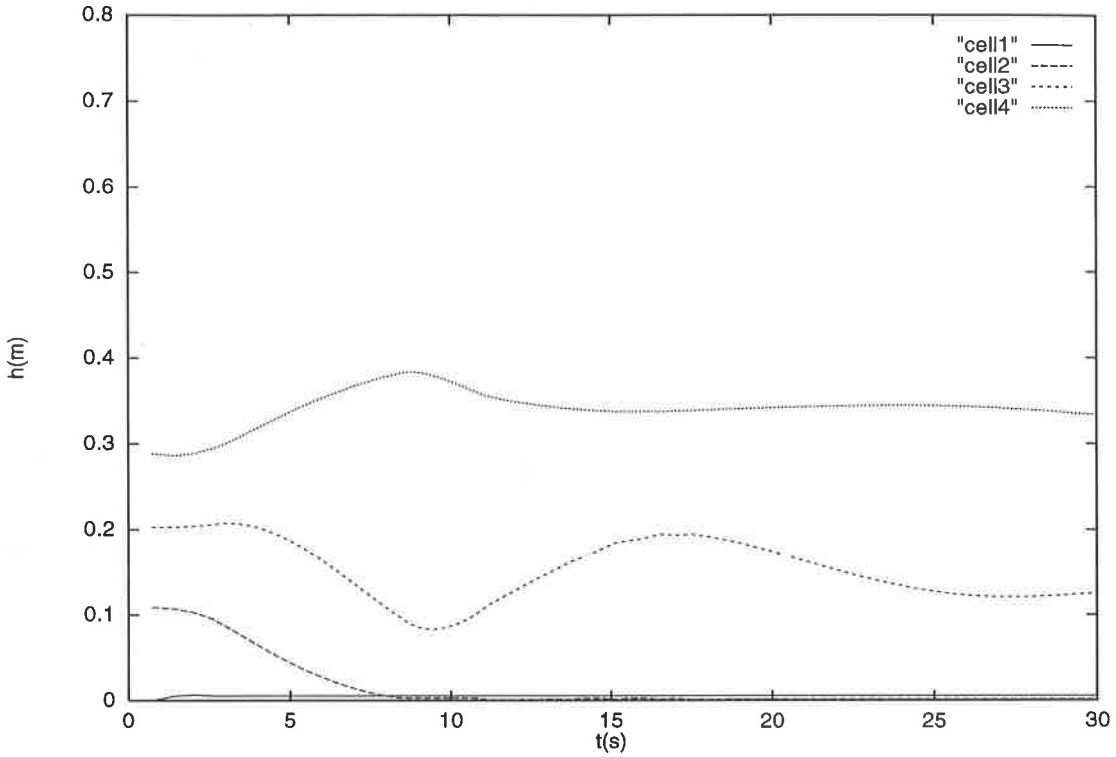

Figure 22: Time evolution of the depth of water in cell1, cell2, cell3 and cell4 in a cross section situated at 47.5m.

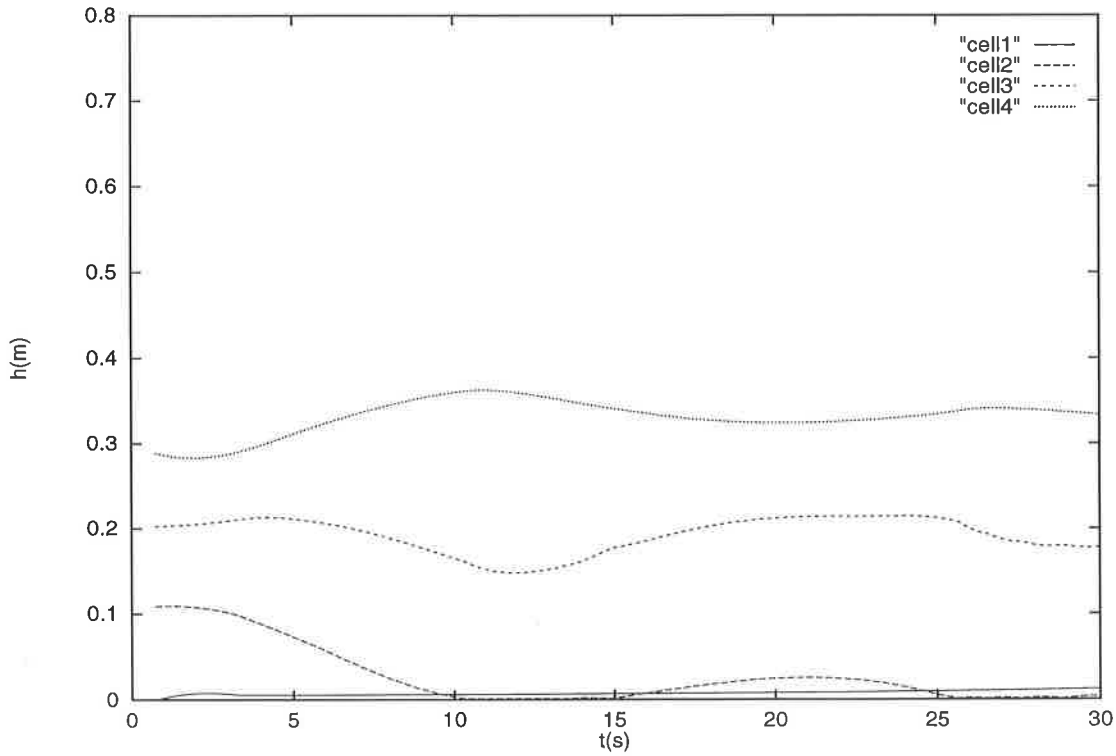

Figure 23: Time evolution of the depth of water in cell1, cell2, cell3 and cell4 in a cross section situated at 97.5m.

6 Conclusions

An efficient first-order multidimensional upwind scheme for the modelling of the Shallow Water system of equations is presented. Of practical interest is its ability to describe easily a wide range of problems such as complex flow domains, basin irrigation problems and problems involving wetting/drying, as we have shown in this work.

A numerical test, the simulation of a dam-break problem in an L-shaped channel, has been compared with experimental data to validate and explore the limitations of the scheme, as well as the difference between using quadrilateral or triangular unstructured meshes.

In future work we intend to extend the scheme to second order in both space and time in order to achieve better accuracy, and make some comparisons to determine the influence of the number of nodes and cells used in each case and the CFL constraint.

The results produced in the infiltration problem are strongly influenced by the initial conditions and the friction terms. We will study other possibilities to overcome this problem in order to have better approximations to reality. Our first step will be the study of the upwind treatment of the source terms.

Finally, the wetting/drying problem is presented and the concept of time-dependent internal boundaries is defined with the description of the possible situations that can occur. Some results involving different inflow boundary conditions (line inflow and corner inflow) are presented. We intend to apply this approach to a real case.

7 Acknowledgements

The author wants to express her gratitude to the members of the Numerical Analysis Group at Reading University in general for their welcome and, in particular, to Prof. Mike Baines and Dr. Matthew Hubbard for their support and many interesting discussions. The work was financed by ESF, Program AMIF (Applied Mathematics for Industrial Flow Problems), whom the author would also like to thank.

References

[1] Abbott M.B., *"Computational Hydraulics"*, Ashgate Pub. Comp., 1992.

[2] Abbott M.B., Cunge J.A., *"Engineering Applications of Computational Hydraulics"*, Pitman Pub., 1982

[3] Akanbi A. A., Katopodes N.D., *"Model for flood propagation on initially dry land"*, Journ. Hydr. Div., Vol 114, n° 7, pp 689-706, ASCE, 1988.

[4] Alcrudo, F., *"Esquemas de lata resolución de variación total decreciente para el estudio de flujos discontínuos de superficie libre"*, Tesis Doctoral, Universidad de Zaragoza, 1992.

[5] Alcrudo, F., García-Navarro P., *"A high resolution Godunov-type scheme in finite volumes for the 2D shallow water equations"*, Int. Journ. for Numerical Methods in Fluids, Vol 16, n° 6, pp 489-505, 1991.

[6] Anderson J.D., Degrez G., Dick E., Grundmann R., *"Introduction to Computational Fluid Dynamics"*, Annual Lecture Series, Von Karman Institute, 1996.

[7] Barley J.J., *"A survey of operator splitting applied to upwind differencing"*, Numerical Analysis Report, 12/88, University of Reading, 1988.

[8] Bellos C.V., Soulis J.V., Sakkas J.G., *"Computing 2-D unsteady open channel flow by finite volume method"*, Proceedings of the VII Intl. Conf. on Computational Methods in Water Resources, 1988.

[9] Bellos C.V., Soulis J.V., Sakkas J.G., *"Computation of two-dimensional dambreak induced flows"*, Adv. in Water Resources, Vol 14, n° 1, pp 31-41, 1991.

[10] Berzins M., Ware J.L., *"Positive cell-centered finite volume discretisation methods for hyperbolic equations on irregular meshes"*, Applied Numerical Mathematics, 1995.

[11] Chow V.T., *Open Channel Hydraulics*, MacGraw-Hill, 1959.

[12] Cunge J.A., Holly F.M., Verwey A., *"Practical aspects of computational river hydraulics"*, Pitman Pub. Inc., 1989.

[13] Fennema R.J., Chaudhry M.H., *"Explicit methods for 2D transient free surface flows"*, Journ. of Hydraulic Engineering, Vol 116, n° 8, pp 1013-1034, ASCE 1990.

[14] Franco A. B., *"Modelacao computacional e experimental de escoamentos provocados por roturas de barragens"*, Tese de Doutoramento, Universidade Técnica de Lisboa, 1996.

[15] Glaister P., *"Difference schemes for the shallow water equations"*, Numerical Analysis Report, 9/87, University of Reading, 1987.

[16] Glaister P., *"Approximate Riemann solutions of the shallow water equations"*, Journ. of Engineering Mathematics, Vol 24, n° 1, pp 45-53, 1990.

[17] García-Navarro P., Hubbard M.E., Priestley A., *"Genuinely multidimensional upwinding for the 2d Shallow Water equations"*, Journ. of Computational Physics, Vol 121, pp. 79-93, 1995.

[18] García-Navarro P., Priestley A., *"A conservative and shape-preserving semi-lagrangian method for the solution of the shallow water equations"*, Int. Journ. for Numerical Methods in Fluids, Vol 18, n° 3, pp 273-294, 1994.

[19] Osher S., Solomon F., *"Upwind difference-schemes for hyperbolic systems of conservation laws"*, Mathematics of Computations, Vol 38, n° 158, pp 339-374, 1982.

[20] Playán E., *"Two-dimensional hydrodynamic simulation of basin irrigation: analysis of field shape effects on irrigation performance"*, PhD Thesis, Utah State University, 1992.

[21] Playán E., Walker W.R., Merkley G.P., *"Two-dimensional simulation of basin irrigation. I: Theory and Validation"*, Journ. Irrig. Drain. Div., ASCE, 1994.

[22] Sleigh P. A., Berzins M., Gaskell P. H., Wright N.G., *"An unstructured Finite-Volume Algorithm for predicting flow in rivers and estuaries"*, Computers and Fluids, 1997.